Bone Reports 5 (2016) 199–207

Contents lists available at ScienceDirect

Bone Reports

journal homepage: www.elsevier.com/locate/bonr

Impaired glucose tolerance attenuates bone accrual by promoting the maturation of osteoblasts: Role of Beclin1-mediated autophagy

E. Rendina-Ruedy [a], J.L. Graef [a], S.A. Lightfoot [b], J.W. Ritchey [c], S.L. Clarke [a], E.A. Lucas [a], B.J. Smith [a,*]

[a] Department of Nutritional Sciences, Oklahoma State University, Stillwater, OK, United States
[b] Center for Cancer Prevention and Drug Development, University of Oklahoma Health Sciences Center, Oklahoma City, OK, United States
[c] Department of Veterinary Pathobiology, Oklahoma State University, Stillwater, OK, United States

ARTICLE INFO

Article history:
Received 20 June 2016
Accepted 7 August 2016
Available online 8 August 2016

Keywords:
Hyperglycemia
Insulin
Macroautophagy
Osteocyte

ABSTRACT

Patients with type 2 diabetes mellitus (T2DM) experience a 1.5–3.5 fold increase in fracture risk, but the mechanisms responsible for these alterations in bone biomechanical properties remain elusive. Macroautophagy, often referred to as autophagy, is regulated by signaling downstream of the insulin receptor. Metabolic changes associated with the progression of glucose intolerance have been shown to alter autophagy in various tissues, but limited information is available in relation to bone cells. The aim of this study was to (a) investigate whether autophagy is altered in bone tissue during impaired glucose tolerance, and (b) determine how autophagy impacts osteoblast differentiation, activity, and maturation. Four-week-old, male C57BL/6 mice were fed a control (Con) or high fat (HF) diet for 2, 8, or 16 wks. Mice on the HF diet demonstrated elevated fasting blood glucose and impaired glucose tolerance. Reduced trabecular bone in the femoral neck was evident in the mice on the HF diet by 8 wks compared to Con mice. Histological evaluation of the tibia suggested that the high fat diet promoted terminal differentiation of the osteoblast to an osteocyte. This shift of the osteoblasts towards a non-mineralizing, osteocyte phenotype appears to be coordinated by Beclin1-mediated autophagy. Consistent with these changes in the osteoblast *in vivo*, the induction of autophagy was able to direct MC3T3-E1 cells towards a more mature osteoblast phenotype. Although these data are somewhat observational, further investigation is warranted to determine if Beclin1-mediated autophagy is essential for the terminal differentiation of the osteoblasts and whether autophagy is having a protective or deleterious effect on bone in T2DM.

1. Introduction

Type 2 diabetes mellitus (T2DM) is a major public health problem in the U.S. affecting ~25 million adults (Centers for Disease Prevention and Control, 2011). The CDC has projected that the prevalence of T2DM will double or even triple, affecting 1 in 3 adults, by 2050 if current trends continue (Centers for Disease Prevention and Control, 2011). In addition to classic complications associated with T2DM, (e.g., peripheral vascular disease, retinopathy, nephropathy, impaired wound healing, and neuropathy) it has recently been established that type 2 diabetics are also at greater risk of fracture, primarily hip fracture, 5–10 years post diagnosis. Furthermore, it was demonstrated that the clinical determinant of fracture risk, bone mineral density (BMD), and the World Health Organization Fracture Risk Algorithm (FRAX) underestimate fracture risk in adults with T2DM (Schwartz et al., 2011). While impaired insulin signaling, alterations in the inflammatory response, and the accumulation of advanced glycation end products (AGEs) have been proposed to contribute to this phenomenon, the mechanism through which the bone metabolic changes are occurring has remained elusive (Ferron et al., 2010; O'Rourke, 2009; Cottam et al., 2004; Smith et al., 2006; McCarthy et al., 1997; Vashishth, 2007). Therefore, to begin to understand why T2DM increases skeletal fragility, it is imperative that alterations in bone metabolism be investigated with increasing duration of hyperglycemia and glucose intolerance.

The hyperglycemia associated with T2DM is attributed, in part, to diminished insulin sensitivity and alterations in the downstream signaling cascade. The resulting alterations in cellular processes have not been extensively investigated in bone cells. Autophagy is one such process that is controlled by proteins downstream of the insulin receptor (IR) and is involved in energy (i.e., glucose) sensing, effectively regulating cell survival or death by means of organelle recycling (Bursch et al., 2008). This

Abbreviations: T2DM, type 2 diabetes mellitus; AGEs, advanced glycation end products; IR, insulin receptor; Atg, autophagy-related proteins; ULK1/2, unc-like kinase; FIP200, focal adhesion; Beclin1, Bcl-2-interacting myosin-like coiled-coil protein; Ambra1, vacuole sorting protein (Vps34/15), activating molecule in Beclin-1 regulator autophagy; UVRAG, ultraviolet radiation resistance-associated gene; PE, phosphatidylethanolamine; LC3, microtubule associated light chain; AIN, American Institute of Nutrition; BafA1, bafilomycinA1; Rap, rapamycin; mTORC1, mammalian or mechanistic target of rapamycin complex; AMPK, adenosine monophosphate-activated protein kinase; ROCK1, rho kinase 1.

* Corresponding author at: Department of Nutritional Sciences, HSci 420, Oklahoma State University, Stillwater, OK 74078, United States.
E-mail address: bjsmith@okstate.edu (B.J. Smith).

http://dx.doi.org/10.1016/j.bonr.2016.08.001

complex, multi-step process involves: 1) initiation characterized by the activation of the initiation complex (ULK1/2, FIP200, and Atg101), 2) membrane nucleation involving Beclin1's association with Vps34/15, Atg14L, Ambra1 or UVRAG, 3) phagophore formation by Atg12, Atg5, and Atg16, 4) sequestration and autophagosome formation facilitated by phosphatidylethanolamine (PE) conjugation of LC3 (LC3-II), 5) followed by degradation via autophagosome-lysosome fusion (Wirth et al., 2013; Tanida et al., 2004; Chan, 2012). Although changes in autophagy have been demonstrated in β-cells, hepatocytes, cardiac myocytes, and adipocytes during diabetes, no published reports have examined whether autophagy is altered in bone cells during the development of impaired insulin sensitivity during impaired insulin sensitivity (Masini et al., 2009; Jansen et al., 2012; Nunez et al., 2013; Ost et al., 2010; Liu et al., 2009). Similar to other mesenchymal-derived cells (e.g., myocytes and adipocytes), bone forming osteoblasts express the IR; therefore, during glucose intolerance, osteoblasts may experience impaired insulin signaling, resulting in the up-regulation of autophagy.

While significant advances in the field of autophagy as it relates to bone have been made in the past 5 yrs., conflicting evidence exists on how alterations in the autophagic process will impact osteoblast differentiation, maturation, and activity. For example, Yang et al. (Yang et al., 2013) described a serum-deprivation model of autophagy utilizing osteoblast-like MC3T3-E1 cells in which growth factors and insulin are absent from the culture and noted increased initiation of autophagy and autophagosome formation as evidenced by increased ULK1, Beclin1, and LC3-II protein expression. Interestingly, when osteoblasts were treated with estradiol, apoptotic events were decreased while autophagy was enhanced (Yang et al., 2013). In this case, autophagy induction by estradiol was associated with a cytoprotective process; however, publications on glucocorticoid treatment and the free fatty acid, palmitate, describe autophagy as a means by which osteoblasts and osteocytes undergo cell death (Gunaratnam et al., 2013; Xia et al., 2010). Two ground-breaking studies related to autophagy and bone have utilized conditional knockout models. Onal et al. (Onal et al., 2013) knocked-out the autophagic protein, Atg7, in terminally differentiated osteocytes (DMP1-Cre). These animals exhibited a decrease in femoral, spinal, and total BMD, which was attributed to a decrease in both trabecular and cortical bone. Further insight into how autophagy impacts bone metabolism was provided in an osteoblast (Osx-Cre) conditional knockout of FIP200, in which the animals demonstrated dramatically lower trabecular and cortical bone at 1, 2, and 6 months of age due to decreased bone formation (Liu et al., 2013). This study also provided evidence that autophagy is up-regulated during osteoblast maturation and terminal differentiation. Together, these two studies demonstrate that basal autophagy promotes osteocyte function, supports nodule formation by osteoblasts and contributes to the terminal differentiation of osteoblasts. Given our recent report that the attenuation of bone formation associated with increasing duration of impaired insulin signaling is primarily attributed to suppressed osteogenesis (Rendina-Ruedy et al., 2015a), alterations in autophagy of the osteoblast my contribute to this skeletal phenotype.

Based on the regulation of autophagy by the insulin signaling pathway, insulin resistance during T2DM may increase autophagy in osteoblasts initially providing protection from cellular stress and, possibly, inducing cellular maturation. While limited literature exists to suggest that autophagy is an important cellular process for osteoblast differentiation and function, no studies have sought to determine how alterations in insulin sensitivity and/or glucose availability in a model of T2DM could impact these cells and the resulting skeletal phenotype. Previous studies in other tissues/cells have also supported the notion that autophagy may act in a biphasic manner, initially protecting cells from stress occurring during reduced insulin sensitivity, while prolonged autophagy could be detrimental (Liu et al., 2013; Eisenberg-Lerner et al., 2009). Therefore, this study was designed to (a) investigate whether autophagy is altered in the bone during the initial development and progression of glucose intolerance; and (b) determine how autophagy impacts osteoblast differentiation, activity, and maturation.

2. Materials and methods

2.1. Animal use and care

Four week old male C57BL/6N mice (Charles Rivers, Wilmington, MA), referred to hereafter as C57BL/6, were utilized for the current study. The rationale for choosing this mouse strain was based on their metabolic and skeletal response to high fat diet, which was more similar to clinical pathophysiology of T2DM versus the C57BL/6J strain (Rendina-Ruedy et al., 2015a). The mice were allowed to acclimate for 1 wk. and then assigned to one of six groups ($n = 8$–10 mice/group) to receive the control (Con; modified AIN-93M, sucrose matched, 10% kcals from fat; Research Diets D12450J) or a high fat (HF; 60% kcals from fat; Research Diets D12492) diet for 2, 8, or 16 wk. Bodyweight and food intake were recorded throughout the study. At each study end point, mice were anesthetized (ketamine/xylazine cocktail 70 and 30 mg/kg body weight, respectively) and exsanguinated via the carotid artery. Plasma was collected by centrifuging whole blood in EDTA-coated tubes for 15 min at 3000 ×*g*. Tibiae and femurs were disarticulated and stripped of surrounding soft tissue. The femurs to be used for microCT were stored in phosphate buffered saline (PBS) at −4 °C, while femurs used for RNA and protein extraction were flushed of their bone marrow and stored in a cryotank (−140 °C). The tibiae were stored in 10% neutral buffered formalin (NBF) until histological processing. All procedures were approved by the Institutional Animal Care and Use Committee of Oklahoma State University.

2.2. Intraperitoneal glucose tolerance test and plasma insulin (IGTT)

Three to five days prior to the termination of each study period, mice were fasted for 6 h and blood glucose was determined at baseline. Mice then received an intraperitoneal injection of glucose solution (2 g glucose/kg body weight) and their blood glucose was monitored at 15, 30, 60, 90, and 120 min. Plasma insulin was also determined at each study end point (i.e., 2, 8 and 16 wks) using a commercially available ELISA kit (Crystal Chem, Downers Grove, IL).

2.3. Determination of alterations in microarchitecture by microCT

Previously, we have reported that impaired trabecular bone acquisition occurs over time in the distal femur metaphysis (Rendina-Ruedy et al., 2015b). In this study, micro-computerized tomography (microCT40, SCANCO Medical, Switzerland) was performed to determine if the compromise in trabecular bone was evident in the proximal femur. Therefore, trabecular bone within the femoral neck was determined by scanning each specimen at a resolution of 2048 × 2048 pixels, pixels, followed by identifying an approximately 280 μm volume of interest (VOI) beginning 30 μm distal to the femoral neck growth plate. Trabecular bone parameters evaluated included bone volume expressed as a percentage of total volume (BV/TV), trabecular number (Tb.N.), trabecular thickness (Tb.Th.), trabecular separation (Tb·Sp.) connectivity density (Conn.Dens.) and structural model index (SMI). All of the acquired images for trabecular and cortical bone were analyzed at a threshold of 340, and a sigma and support of 1.2 and 2.0, respectively.

2.4. Quantification of osteoblasts and osteocytes in the tibia

Fixed tibial samples were processed by exposure to sequential dehydration steps with ethanol, cleared with toluene, and paraffin embedded. Using a Leica RM2165 microtome (Wetzlar, Germany) tibial sections were cut on a longitudinal axis (5 μm each) and then stained with hematoxylin and eosin. Osteoblasts were identified as cuboidal cells (>3 cells) lining the trabecular bone surface (125 μm distal to the growth plate in the tibial metaphyseal region) and osteocytes were distinguished in the tibial cortex located in developed lacuna (Clarke, 2008; Florencio-Silva et al., 2015). Osteoblasts and osteocytes were

enumerated manually in 20 fields (20× magnification; 3–4 slides/animal) and the means were calculated for each animal. Additionally, empty lacunae were counted in the tibial cortex from 30 fields (20× magnification) and quantified similarly.

2.5. Cell culture experiments

Mouse pre-osteoblast MC3T3-E1 cells (Riken BioResource Center, Ibaraki, Japan) were maintained in complete αMEM containing 10% fetal bovine serum (FBS), 100 U/L penicillin G and 100 mg/L streptomycin, and 2 mM L-glutamine at 37 °C in a humidified atmosphere of 5% CO_2. For osteoblast differentiation experiments, osteogenic medium containing complete αMEM supplemented with 10 mM β-glycerophosphate and 25 μg/mL ascorbic acid was used. Rapamycin was used for the induction of autophagy (Noda & Ohsumi, 1998; Sarbassov et al., 2005; Kim et al., 2002) while bafilomycin A1 (BafA1) was used to prevent the lysosomal degradation of LC3-II (Yamamoto et al., 1998) (Cayman Chemical Company, Ann Arbor, MI), and both were dissolved in DMSO purged with N_2 according to the manufacture's specifications.

Undifferentiated pre-osteoblastic MC3T3-E1 cells were plated (1.0×10^6 cells/cm^2) and allowed to adhere for 24 h in complete αMEM (i.e., 0 day differentiation). Cells were then treated with 0 μM (Con and DMSO) or 10 μM rapamycin for 24 h. Due to the lysosomal degradation of LC3B-II protein 0 or 200 nM of BafA1 was added to cultures 2 h prior to RNA and protein harvest (e.g., 22 h). To determine changes induce by autophagy in a more mature osteoblast, osteogenic medium was added to MC3T3-E1 cultures, and cells were allowed to differentiate for 7 days. Following this differentiation period, cells were treated with 0 or 10 μM rapamycin for 24 h, while BafA1 was added 2 h before the RNA and protein was extracted.

2.6. RNA extraction and qPCR analyses

Total RNA was extracted from pulverized, flushed femurs (Spex 6770 Freezer Mill, Metuchen, NJ) and MC3T3-E1 cells using TriZol Reagent (Life Technology, Rockville, MD), following the manufacturers' protocol. RNA was quantified using a Nanodrop Spectrophotometer (Rockland, DE) while gel electrophoresis was carried out to verify the quantity and quality of all RNA samples. cDNA was synthesized using 2 μg of total RNA pre-treated with DNase I and subjected to reverse-transcription (Superscript II, Invitrogen, Carlsbad, CA). Each qPCR reaction was performed in duplicate or triplicate using SYBR green chemistry (SABiosciences, Valencia, CA) on the Applied Biosystems 7900HT Fast Real-Time PCR System (Foster City, CA). All qPCR results were evaluated by the comparative cycle number at threshold (C_Q) method (User Manual #2, Applied Biosystems), using peptidylprolyl isomerase B (*Ppib*) as the invariant control. Primer sets for target genes can be found in Supplemental materials (Supp Table 1).

2.7. Protein extraction and western blot analyses

Crude protein was prepared from femur tissues (i.e., bone marrow flushed) and MC3T3-E1 cells. Both the pulverized femur and MC3T3-E1 cells were lysed using RIPA buffer containing a protease/phosphatase inhibitor cocktail (Cell Signaling Technologies, Dancers, MA). Lysates were incubated on ice for 40 min, with vortexing and sonication every 10 min. Samples were then centrifuged at 16,000 ×*g* for 15 min at 4 °C. Supernatant containing total protein was then aliquoted and stored at −80 °C. Prior to western blot analyses, protein concentration was determined by bicinchoninic acid (BCA) assay. Immunoblots were probed with primary antibodies targeted against Beclin1 (Novus Biologicals, Littleton, CO), pBeclin1 (EMD Millipore, Billerica, MA), β-Actin (Santa Cruz Biotechnology, Dallas, TX), and LC3B and ROCK1 (Cell Signaling Technology, Danvers, MA).

2.8. Statistical analyses

Statistical analyses were accomplished using SAS Version 9.3 (SAS Institute, NC). Comparisons were made between dietary treatment groups across all time points using two-way ANOVA, followed by post hoc analysis with Fischer's least square means separation test when F values were significant ($P < 0.05$), unless otherwise stated. Results from the IGTT at each study endpoint (i.e., 2, 8, or 16 wk) were analyzed separately by performing student's paired *t*-test to determine differences between the Con and HF groups at a given time point following glucose administration (i.e., 15, 30, 60, 90, 120 min). In vivo, femur western blot data were analyzed using a Wilcoxon signed-rank test due to lack of normality between Con and HF diet groups at a given time point. For in vitro experiments comparisons were made at a given time between treatment groups and therefore, one-way ANOVA was performed followed by post hoc analysis with Fischer's least square means separation test when F values were significant ($P < 0.05$).

3. Results

3.1. Metabolic and skeletal changes occurring in response to a high fat diet with time

Mice on the HF diet exhibited elevated fasting blood glucose at the 2, 8, and 16 wk. time points (Fig. 1A). At the 2-wk. time point, mice on the HF diet were hypoinsulinemic (Con = 206.4 pg/mL; HF = 148.0 pg/mL; *P*-value = 0.0025). No difference in fasting plasma insulin was evident between dietary treatment groups at 8 wk. (Con = 248.9 pg/mL; HF = 257.3 pg/mL; *P*-value = 0.8342), but after 16 wk. the mice on the HF diet demonstrated elevated plasma insulin (Con = 370.8 pg/mL; HF = 736.7 pg/mL; *P*-value = 0.0159). At 2 wk. (Fig. 1B) and 8 wk. (Fig. 1C) mice on the HF diet were able to restore blood glucose to some extent by the 120 min time point of the IGTT which is associated with impaired glucose tolerance or pre-diabetes. However, given the results of the IGTT at 16 wk., it was evident that mice on the HF diet were unable to restore blood glucose by the IGTT final time point, despite elevated insulin (Fig. 1D). Therefore, mice at the 2 and 8 wk. time point on the HF diet demonstrated metabolic changes corresponding to pre-diabetes, while the metabolic response was more advanced at the later 16 wk. time point (i.e., hyperglycemia, hyperinsulinemia, and glucose intolerance).

Trabecular BV/TV in the femoral neck was unchanged after 2 wk. on the HF diet compared to the Con; however, mice on the HF diet for 8 and 16 wk. exhibited significantly less trabecular bone compared to Con mice (Table 1). Although peak trabecular bone mass was achieved in the Con mice at the 8 wk. experimental time point (or 13-wk.- old mice), it was evident that trabecular bone deposition did not continue at a normal rate after 2 wk. on the HF diet (Supp Fig. 1). A similar trend was observed in Tb.Th., Conn.Dens., and SMI, indicative of a structurally weaker bone (Table 1). Cortical bone (i.e., cortical thickness) was previously shown to be reduced by 7.4% at the femur mid-diaphysis (Rendina-Ruedy et al., 2015b).

Interestingly, histological evaluation of the proximal tibia metaphysis in the 2 wk. Con group contained a large number of cuboidal-shaped, active osteoblasts (Clarke, 2008; Florencio-Silva et al., 2015), whereas the mice on the HF diet exhibited a dramatic decrease in osteoblasts (Fig. 2A and B). To be expected, osteoblast number decreased with age (e.g., 7, 13, and 21 wk. of age) in the Con mice; however, the lowest number of osteoblasts was observed in the mice on a HF diet for 8 and 16 wk. (Fig. 2B). While these results were somewhat expected given the decrease in trabecular bone volume, the animals on the HF diet had a higher number of osteocytes at 2, 8, and 16 wk., compared to their respective controls (Fig. 2C). Taken together, these data suggest that the HF diet accelerated osteoblast terminal differentiation to an osteocyte. Although artifacts can be problematic when performing histomorphometry on paraffin

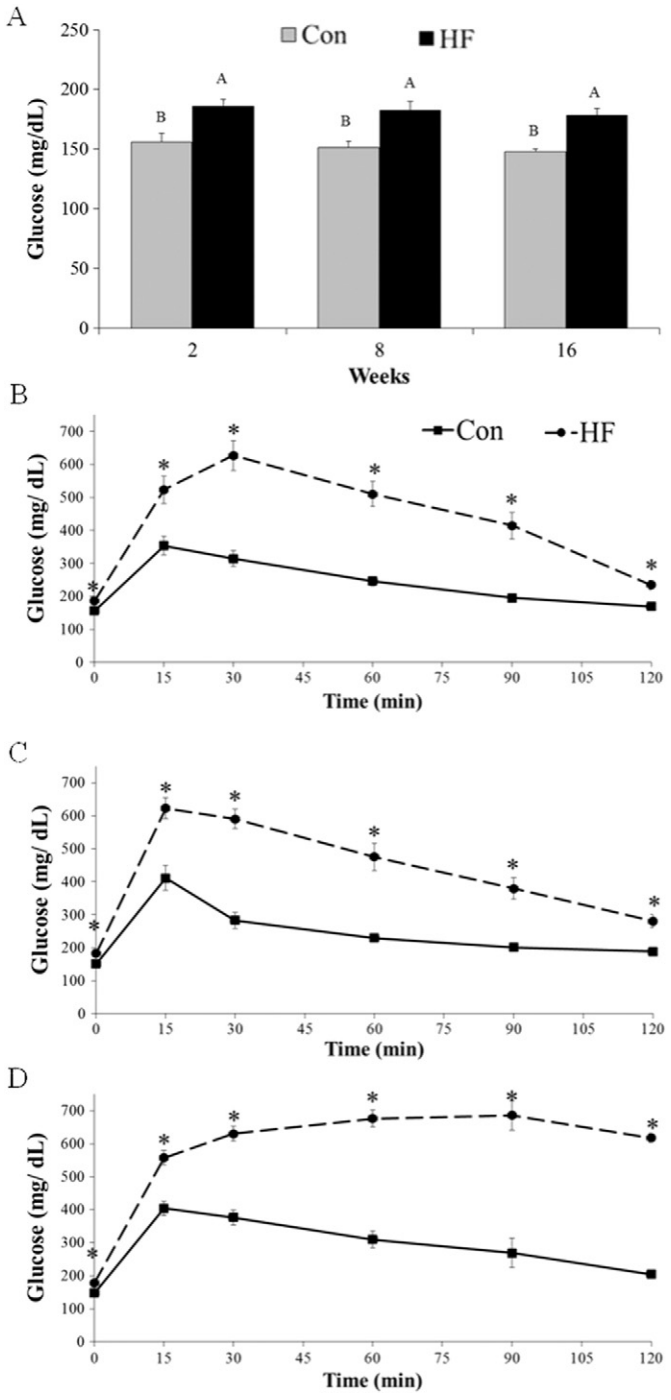

Fig. 1. Fasting (6 h) blood glucose (A) was determined prior to the administration of the intraperitoneal glucose tolerance test (IGTT). IGTT was performed by injecting (IP) glucose *solution* (2 g glucose/kg bodyweight) and tracking blood glucose in mice that were maintained on a control (Con; AIN93M) or high fat (HF; 60% kcal from fat) for 2 (B), 8 (C), and 16 (D) wk. Data are presented as the mean ± SE. Changes in fasting blood glucose were determined by 2-way ANOVA to compare Con vs. HF at each study endpoint while student's paired *t*-test was used to determine differences between the Con and HF groups at a given time point following glucose administration (i.e., 15, 30, 60, 90, 120 min). Bars that share the same superscript letter are not significantly different from each other ($P < 0.05$), while the symbol * represents a significant difference ($P < 0.05$) between dietary treatments at a given time point during the IGTT (Student's paired *t*-test).

embedded bone, we did document an number of empty lacunae in the cortex of mice on the HF diet at 2 and 8 wk., and these changes were more pronounced at the 16 wk. time point (Fig. 2D).

3.2. Determination of altered autophagy in bone during HF diet

To test the hypothesis that autophagy is up-regulated during HF diet-induced metabolic derangements and contributing to the induction of osteoblast maturation, proteins involved in autophagy regulation were quantified in the femur (Fig. 3A). Interestingly, the autophagy-specific post-translational modification of Beclin1, pBeclin1 (Thr119), protein abundance was shown to be the higher in the 8 wk. HF group (Fig. 3A). No changes were observed in LC3B-II protein abundance over time and in response to diet, but this was predicted as LC3B-II was presumably degraded in the lysosome (Fig. 3A). Although alterations were noted in pBeclin (Thr119), no changes were observed in ROCK1, a kinase responsible for this site-specific phosphorylation (Fig. 3A).

Gene expression analyses revealed that while no changes were observed in *Maplc3a* (Fig. 3B) and *Maplc3b* (Fig. 3C), *Becn1* (Fig. 3D) was up-regulated after 2 wk. on HF diet, preceding the changes in pBeclin1 protein abundance. Furthermore, autophagy induction after 2 and 8 wk. of HF diet appears to lower apoptosis given the *Casp3* mRNA abundance, while apoptotic events appear to be elevated in the bone due to prolonged HF diet feeding (Fig. 3E).

3.3. In vitro model of autophagy induction and transcriptional regulation of osteoblastogenesis

To determine how the up-regulation of autophagy with glucose intolerance affects osteoblastogenesis, MC3T3-E1 cells were cultured with 10 μM rapamycin with the addition of 200 nM BafA1 for the last 2 h of the experiment to inhibit lysosomal degradation. Although it appears that immature (Fig. 4A) and mature osteoblasts (Fig. 4B) have high levels of basal autophagy based on the abundance of LC3B-II in control cells (i.e., Con and DMSO-vehicle control), the addition of 10 μM rapamycin for 24 h was able to increase autophagy as evidenced by increased levels of LC3-II protein (Fig. 4C) and *Maplc3a* (Fig. 4D) and *Maplc3b* (Fig. 4E) mRNA. However, no changes were observed in *Becn1* mRNA or protein abundance of pBeclin1 or Beclin1 in undifferentiated (0 d) or differentiated (7 d) MC3T3-E1 cells (*data not shown*).

With this model of autophagy induction in the osteoblast was established, genes involved in osteoblast differentiation, activity, and maturation were determined. Immature, osteoblast MC3T3-E1 cells undergoing autophagy induced via rapamycin treatment demonstrated decreased levels of mRNA for genes critical for osteoblast differentiation and early osteoblast activity including *Atf4* (Fig. 5D), *Cbfa1* (Fig. 5E), *Alpl* (Fig. 5F), and *Col1a* (Fig. 5G). Conversely, an up-regulation was noted in the cell cycle regulator *Ccnd1* (Fig. 5A) and the gene that encodes osteopontin, *Spp1*, an indicator of late osteoblast activity (Fig. 5H). While a similar pattern was observed when autophagy was up-regulated in a more mature osteoblasts (i.e., 7 day differentiation), *Ccnd1* mRNA (Fig. 5A) was lower in the rapamycin- treated group compared to controls (Con and DMSO) and no changes were observed in *Cbfa* (Fig. 5E), *Alpl* (Fig. 5F) and *Col1a1* (Fig. 5G). In these more mature osteoblasts, a significant increase in osteocalcin gene expression (*Bglap*) was also noted (Fig. 4). The differences in the regulation of these genes are presumably indicative of the difference in transcriptional machinery essential during the different stages of osteoblastogenesis. However, in both the undifferentiated and differentiated MC3T3-E1 cells, enhanced autophagy appears to drive the osteoblast towards a more mature phenotype.

4. Discussion

These data demonstrate that during the onset and progression of impaired glucose tolerance and diminished insulin sensitivity, trabecular bone accrual is attenuated in the femoral neck, but to a lesser extent than we have previously reported in the distal femur (Rendina-Ruedy et al., 2015b). This phenotype is observed concurrently with alterations in osteoblast maturation and up-regulated autophagy. These findings

Table 1
Alterations in trabecular microarchitecture of the femoral neck after 2, 8, and 16 wk.

	2 Week		8 Week		16 Week		*P*-value		
	Con	HF	Con	HF	Con	HF	Diet	Time	Diet * time
BV/TV (%)	39.1 ± 1.8^{B}	41.2 ± 3.4^{B}	58.6 ± 3.7^{A}	45.4 ± 3.0^{B}	54.8 ± 2.7^{A}	46.7 ± 1.7^{B}	0.0077	0.0002	0.0323
Tb.N. (1/mm)	8.7 ± 0.2	8.8 ± 0.2	8.8 ± 0.3	8.4 ± 0.3	8.1 ± 0.2	7.6 ± 0.2	0.1576	0.0018	0.5284
Tb.Th. (μm)	56.3 ± 1.9^{E}	60.2 ± 2.9^{DE}	80.8 ± 4.9^{AB}	66.5 ± 2.4^{CD}	85.7 ± 4.6^{A}	74.6 ± 1.8^{BC}	0.013	<0.0001	0.0254
Tb. Sp. (μm)	101.5 ± 2.7	99.3 ± 4.9	89.7 ± 4.5	100.8 ± 7.0	102.1 ± 4.9	112.3 ± 3.1	0.1233	0.0500	0.3289
ConnDens ($1/mm^3$)	453.3 ± 33.5	404.3 ± 21.2	253.6 ± 13.2	284.3 ± 24.4	179.2 ± 14.3	215.7 ± 8.7	0.7223	<0.0001	0.0834
SMI	0.56 ± 0.13^{A}	0.41 ± 0.33^{AB}	-1.73 ± 0.36^{C}	-0.28 ± 0.23^{BD}	-1.10 ± 0.23^{C}	-0.44 ± 0.11^{D}	0.0021	<0.0001	0.0105

MicroCT analyses of trabecular bone in the femoral neck at 2, 8, and 16 weeks on a control (Con = 10% kcal from fat) or HF (60% kcal from fat) diet. Trabecular parameters includes bone volume/total volume (BV/TV), trabecular number (Tb.N.), thickness (Tb.Th.), and separation (Tb·Sp), as well as connectivity density (ConnDens) and structural model index (SMI). Values are expressed as mean ± SE. Data were analyzed using two-way ANOVA. Values within a given row that share the same superscript letter are not significantly different from each other ($P < 0.05$).

suggest that autophagy could be driving the terminal differentiation of osteoblasts towards a non-mineralizing cell, via a Beclin1-mediated mechanism. While bone accrual was unchanged through the first 2 wk., trabecular bone formation was diminished as impaired glucose tolerance progressed. These microarchitectural changes from the femoral neck are consistent with our previous observations in this model that bone formation was attenuated in the distal femoral metaphysis (Rendina-Ruedy et al., 2015b). Although it has been shown by our lab and others that hyperglycemia attenuates bone accrual due to decreased osteoblast differentiation (Rendina-Ruedy et al., 2015b; Lu et al., 2013), the mechanisms involved and the fate of the osteoblasts has not been fully explored. Histological evaluation of the proximal tibia revealed that while osteoblast number and activity was apparently decreased during glucose intolerance, it appeared that osteocyte numbers were increased in these young animals. Although its lineage is derived from an osteoblast, the primary role of the osteocyte is to function as a mechanosensing cell, and as such, is not suspected to mineralize a substantial amount of bone (Lanyon, 1993; Bonewald, 2011). While a more comprehensive evaluation of dynamic and static bone histomorphometry is warranted, these data suggest that the apparent increase in osteocyte number during the initiation of glucose intolerance was driven by the up-regulation of osteoblast maturation, ultimately, impairing bone formation.

The possible rationale for a scenario of increased autophagy contributing to osteoblast maturation is two-fold. First, due to the control of autophagy by proteins involved in insulin signaling and intracellular energy sensors (e.g., mTORC1 and AMPK) this process could be altered during varying degrees of insulin sensitivity/signaling (Masini et al.,

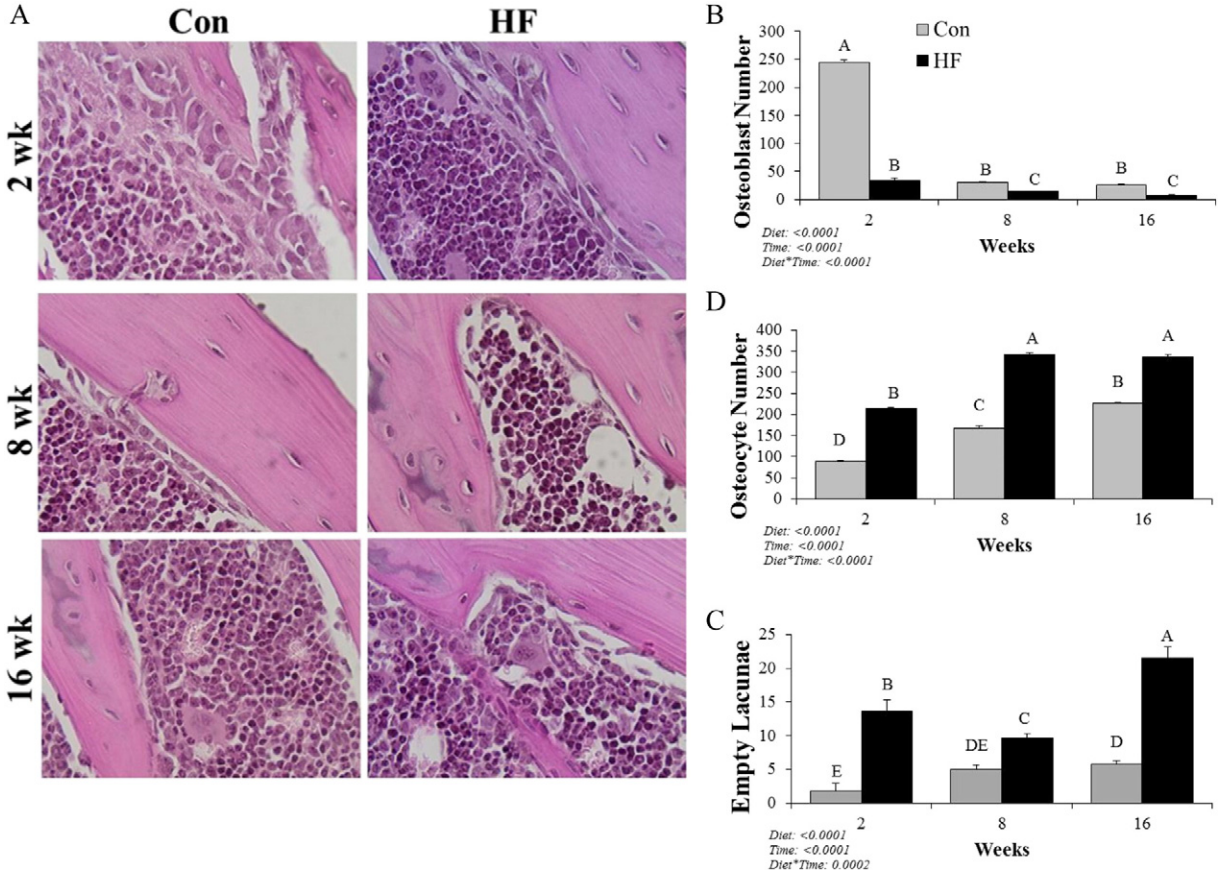

Fig. 2. Representative images of hematoxylin and eosin (H&E) stained tibiae are shown (A) osteoblast (B), osteocyte (C) numbers, and empty lacunae (D) were quantified from 20 fields in control (Con; AIN93M) or high fat (HF; 60% kcal from fat) at the 2, 8, and 16 wk. study endpoints. The data were analyzed by two-way ANOVA, followed by post hoc analysis with Fischer's least square means separation test when F values were significant ($P < 0.05$). Superscripts indicate the diet * time interaction and bars that share the same superscript letter are not significantly different from each other ($P < 0.05$).

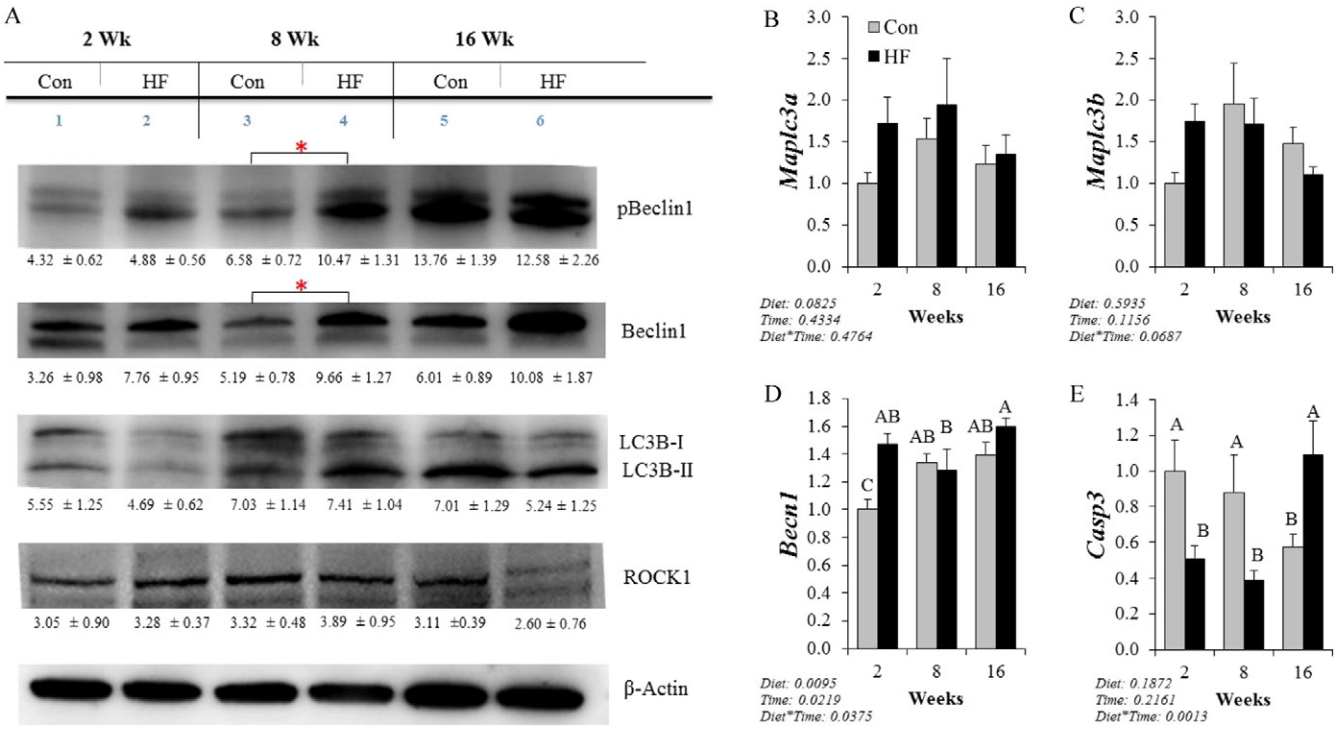

Fig. 3. Western blot analyses and qPCR was performed to determine changes in proteins and genes involved in autophagy from bone samples from mice fed a control (Con; AIN93M) or high fat (HF; 60% kcal from fat) for 2, 8, and 16 wk. Representative images ($n = 5$) of western blots probed for Beclin1, pBeclin1 (Thr119), LC3B, ROCK1 and β-Actin (A). Quantification of Beclin1 (B), pBeclin1 (C), LC3B-II (D), and ROCK1 (E) was carried out by determining density light units (DLU) for a given protein, and expressed normalized back to β-Actin ($n = 5$). Due to lack of normality, these data were analyzed at a given time point using the Wilcoxon rank test. Data are represented as average DLU ± standard error, and symbol * indicates significance ($P < 0.05$). qPCR results for *Maplc3a* (F), *Maplc3b* (G), *Becn1* (H), and *Casp3* (I) were normalized to peptidylprolyl isomerase B (*Ppib*) and expressed as relative mRNA abundance ($n = 6$). Data were analyzed by two-way ANOVA, followed by post hoc analysis with Fischer's least square means separation test when F values were significant ($P < 0.05$). All data are presented as mean ± standard error (SE). Superscripts indicate the diet*time interaction and bars that share the same superscript letter are not significantly different from each other ($P < 0.05$).

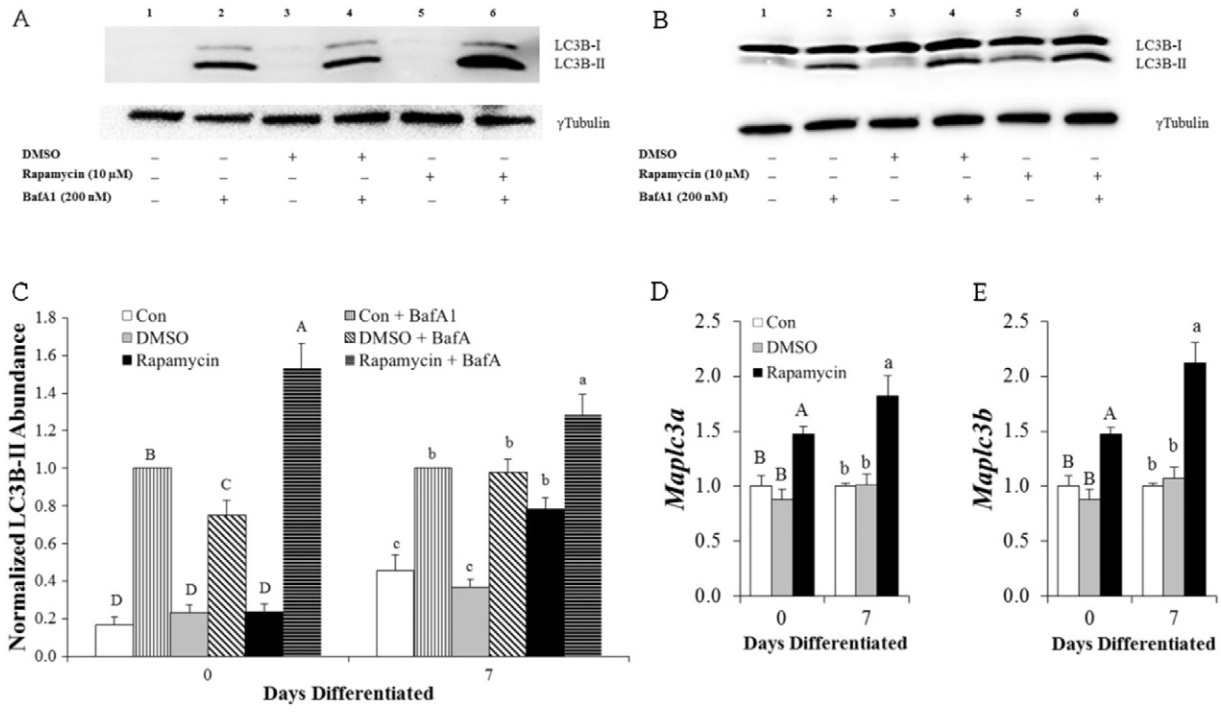

Fig. 4. An in vitro model of increased autophagy in undifferentiated (0 d) and differentiated (7 d) osteoblast was developed by subjecting MC3T3-E1 cells to treatment with 0 μM (Con and DMSO) or 10 μM rapamycin for 24 h. 200 nM bafilomycin (BafA1) of was added to cultures 2 h prior (e.g., 22 h) to protein and RNA extraction. Representative images of western blot analyses of LC3B-II abundance from undifferentiated (A) and differentiated (B) MC3T3-E1 cells are shown. LC3B-II protein abundance was determined by quantifying density light units (DLU) normalized to γ-tubulin DLU (C). qPCR analysis of *Maplc3a* (D) and *Maplc3b* (E), normalized to peptidylprolyl isomerase B (*Ppib*) and expressed as relative mRNA abundance. Data is presented as the mean ± SE ($n = 3$). Data were analyzed by performing one-way ANOVA. followed by post hoc analysis with Fischer's least square means separation test when F values were significant ($P < 0.05$). Bars that share the same superscript letter are not significantly different from each other ($P < 0.05$).

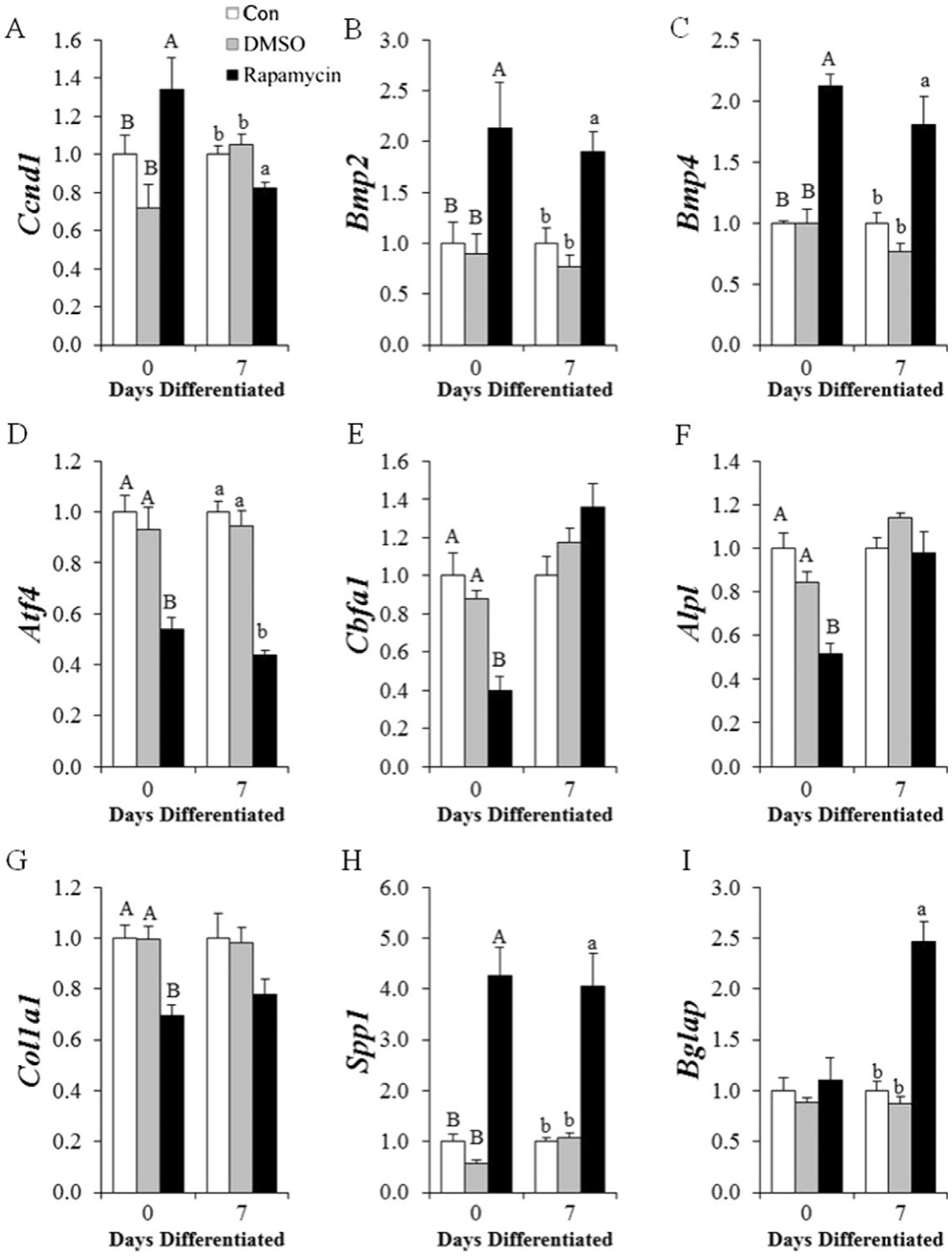

Fig. 5. To determine how autophagy would impact osteoblast differentiation, activity and maturation undifferentiated (0 d) and differentiated (7 d), MC3T3-E1 cells were treated with 0 μM (Con and DMSO) or 10 μM rapamycin for 24 h. RNA was extracted and qPCR was performed to characterize alterations in genes of interest, including; *Ccnd1* (A), *Bmp2* (B), *Bmp4* (C), *Atf4* (D), *Cbfa1* (E), *Alpl* (F), *Col1a1* (G), *Spp1* (H), and *Bglap* (I). All qPCR results were evaluated by the comparative cycle number at threshold (C_Q) method, and genes of interest were normalized to the invariant control, peptidylprolyl isomerase B (*Ppib*) and expressed as relative mRNA abundance. Data is presented as the mean ± SE ($n = 6$). Data were analyzed using one-way ANOVA at a given time point (0 or 6 days) bars that share the same superscript letter are not significantly different from each other ($P < 0.05$).

2009; Ost et al., 2010; Chen et al., 2011). Second, autophagy has been suggested to be essential in the terminal differentiation of osteoblasts to osteocytes (Liu et al., 2013; Nollet et al., 2014). While, one of the most widely accepted indicators of autophagosome formation is LC3-II protein abundance, a major limitation in using this method is that LC3-II is readily degraded in the lysosome, making in vivo assessment a challenge (Mizushima & Yoshimori, 2007). Due to these limitations, Beclin1 protein expression was determined given its recently identified function as a key regulator of membrane nucleation and autophagosome formation (Wirth et al., 2013). Beclin1 protein was shown to be elevated in the femur following the more prolonged periods of glucose intolerance. Beclin1 has been demonstrated to regulate autophagy by its existence in pro-autophagic complexes including Barkor-Vps34-Vps15-Beclin1-AMBRA and Vps34-Vps15-Beclin1-Bif-1-UVRAG, whereas Rubicon bound Vps34-Vps15-Beclin1-UVRAG complex negatively functions in autophagosome maturation (Kang et al.,

2011). Given the multi-functionality of Beclin1, elevated pBeclin1 (Thr119) was identified to be a specific indicator of autophagy activation in the flushed femur of mice fed a HF diet for 8 wks. While the stabilization of pBeclin1 at the 16 wk. time point was somewhat unexpected, given the autophagy-apoptosis axis (Eisenberg-Lerner et al., 2009), these data could indicate that prolonged autophagy in these cells has shifted the cellular response towards cell death by means of apoptosis. Active ROCK1 has been previously described to phosphorylate Beclin1 at Thr119, up-regulating Beclin1-mediated autophagy by dissociating the Beclin1-Bcl-x_L complex (Gurkar et al., 2013). Moreover, ROCK1 kinase activity has been shown to be altered during T2DM, making it a suitable protein of interest in the current model (Lee et al., 2014; Lee et al., 2009). Although, no changes were observed in ROCK1 protein abundance, ROCK1's activity was not assessed and may still provide an explanation for the up-regulated Beclin1-mediated autophagy in this model. Lastly, the fact that no changes were observed in LC3B-II protein levels in the current study, in conjunction with the changes occurring in Beclin1 and *Maplc3a, Maplc3b*, suggests an increase in autophagic flux or the degradation and turnover of sequestered cargo. Therefore, autophagy appears to be increased in response to diminished insulin sensitivity and/or hyperglycemia in osteoblasts and osteocytes; however, a prolonged hyperglycemic state results in apoptosis of these cells.

The up-regulation of autophagy in osteoblast-like MC3T3-E1 cells resulted in their maturation and terminal differentiation. This in vitro model was able to confirm some of the changes occurring in the femur which was important because the bone tissue preparations could still represent a heterogeneous cell population. Moreover, our in vitro conclusions that autophagy induction enhances osteoblast differentiation are further supported by Huang et al., who recently demonstrated that rapamycin increased nodule formation by Alizarin staining (Huang et al., 2015). While we attempted to enrich for osteoblast and osteocyte cell populations by flushing the bone marrow, these cells are expected to be at different stages of differentiation, ranging from osteoblast progenitor cells, to terminally differentiated osteocytes. This difference in cell populations from the femoral samples versus the isolated MC3T3-E1 cells may account for some of the discrepancies in our observations. For instance, the mechanism for autophagy induction in impaired glucose tolerance in the bone appeared to involve a different mechanism than rapamycin-induced autophagy in the MC3T3-E1 cells. Beclin1 mediated autophagy has previously been reported to be a critical mechanism occurring with glucose deprivation in mouse embryonic fibroblasts (MEFs), and not essential for autophagy initiated by rapamycin (Kim et al., 2013). Furthermore, the addition of BafA1 to the MC3T3-E1 cell cultures allowed for the reliable visualization and quantification LC3B-II, however, no lysosomal inhibitor was used in vivo. While these limitations could explain some of the differences between the in vivo and in vitro data, both experimental models provided consistent evidence that the up-regulation of autophagy shifts the osteoblast towards a more mature phenotype.

This study is the first to suggest that impaired insulin sensitivity and hyperglycemia contribute to the dysregulation of bone metabolism by up-regulating autophagy in osteoblasts, directing these cells towards non-mineralizing osteocytes, and ultimately attenuating bone formation. Further investigation is warranted to determine if Beclin1-mediated autophagy is essential for the terminal differentiation of the osteoblasts and whether the promotion of autophagy during T2DM results in lower bone volume. Moreover, given the biphasic nature of autophagy (i.e., cytoprotective vs. cell death), it may be possible that this process exerts different mechanisms on these bone cells resulting in different alterations in bone structure and/or biomechanics. While it is speculated that altered autophagy occurs during glucose intolerance as a result of impaired insulin signaling and/or intracellular glucose availability, further studies are warranted to determine the precise mechanism(s). Additionally, we also acknowledge that bone turnover is a highly sophisticated, coupled process involving not only the osteoblasts and osteocytes, but also the osteoclasts which may also be contributing to the bone phenotype. However, due to the accelerated rate of bone accrual occurring in these young mice, we believe the alterations occurring in the osteoblast outlined herein are of importance. The novel concept that impaired bone formation can result from driving the osteoblast towards a more mature, non-mineralizing phenotype emphasizes the need to better understand the fate and lifespan of osteoblasts, which could have significant clinical implications.

Supplementary data to this article can be found online at http://dx.doi.org/10.1016/j.bonr.2016.08.001.

Conflicts of interest

None.

Acknowledgements

We would like to express our gratitude to Sandra Peterson (Department of Nutritional Sciences, Oklahoma State University, Stillwater, OK 74078) for her technical assistance.

Funding for this project was provided by the United States Department of Agriculture (2012-67011-19906) and Oklahoma Center for the Advancement of Science and Technology (HR10-068) for the funding of the current work.

References

Bonewald, L.F., 2011 Feb. The amazing osteocyte. J. Bone Miner. Res. 26 (2), 229–238.
Bursch, W., Karwan, A., Mayer, M., et al., 2008 Dec 30. Cell death and autophagy: cytokines, drugs, and nutritional factors. Toxicology 254 (3), 147–157.
Centers for Disease Prevention and Control, 2011. National Diabetes Fact Sheet.
Chan, E.Y., 2012 Sep 1. Regulation and function of uncoordinated-51 like kinase proteins. Antioxid. Redox Signal. 17 (5), 775–785.
Chen, Z.F., Li, Y.B., Han, J.Y., et al., 2011 Jan. The double-edged effect of autophagy in pancreatic beta cells and diabetes. Autophagy 7 (1), 12–16.
Clarke, B., 2008 Nov. Normal bone anatomy and physiology. J Am Soc Nephrol]–>Clin. J. Am. Soc. Nephrol. 3 (Suppl. 3), S131–S139.
Cottam, D.R., Mattar, S.G., Barinas-Mitchell, E., et al., 2004 May. The chronic inflammatory hypothesis for the morbidity associated with morbid obesity: implications and effects of weight loss. Obes. Surg. 14 (5), 589–600.
Eisenberg-Lerner, A., Bialik, S., Simon, H.U., et al., 2009 Jul. Life and death partners: apoptosis, autophagy and the cross-talk between them. Cell Death Differ. 16 (7), 966–975.
Ferron, M., Wei, J., Yoshizawa, T., et al., 2010 Jul 23. Insulin signaling in osteoblasts integrates bone remodeling and energy metabolism. Cell 142 (2), 296–308.
Florencio-Silva, R., Sasso, G.R., Sasso-Cerri, E., et al., 2015. Biology of bone tissue: structure, function, and factors that influence bone cells. Biomed. Res. Int. 2015, 421746.
Gunaratnam, K., Vidal, C., Gimble, J.M., et al., 2013 Oct 29. Mechanisms of Palmitate-Induced Lipotoxicity in Human Osteoblasts. Endocrinology.
Gurkar, A.U., Chu, K., Raj, L., et al., 2013. Identification of ROCK1 kinase as a critical regulator of Beclin1-mediated autophagy during metabolic stress. Nat. Commun. 4, 2189.
Huang, B., Wang, Y., Wang, W., et al., 2015 Aug. mTORC1 prevents preosteoblast differentiation through the notch signaling pathway. PLoS Genet. 11 (8), e1005426.
Jansen, H.J., van, E.P., Koenen, T., et al., 2012 Dec. Autophagy activity is up-regulated in adipose tissue of obese individuals and modulates proinflammatory cytokine expression. Endocrinology 153 (12), 5866–5874.
Kang, R., Zeh, H.J., Lotze, M.T., et al., 2011 Apr. The Beclin1 network regulates autophagy and apoptosis. Cell Death Differ. 18 (4), 571–580.
Kim, J., Kim, Y.C., Fang, C., et al., 2013 Jan 17. Differential regulation of distinct Vps34 complexes by AMPK in nutrient stress and autophagy. Cell 152 (1–2), 290–303.
Kim, D.H., Sarbassov, D.D., Ali, S.M., et al., 2002 Jul 26. mTOR interacts with raptor to form a nutrient-sensitive complex that signals to the cell growth machinery. Cell 110 (2), 163–175.
Lanyon, L.E., 1993. Osteocytes, strain detection, bone modeling and remodeling. Calcif. Tissue Int. 53 (Suppl. 1), S102–S106.
Lee, S.H., Huang, H., Choi, K., et al., 2014 Feb. ROCK1 isoform-specific deletion reveals a role for diet-induced insulin resistance. J Physiol Endocrinol Metab]–>Am. J. Physiol. Endocrinol. Metab. 306 (3), E332–E343.
Lee, D.H., Shi, J., Jeoung, N.H., et al., 2009 May 1. Targeted disruption of ROCK1 causes insulin resistance in vivo. J. Biol. Chem. 284 (18), 11776–11780.
Liu, F., Fang, F., Yuan, H., et al., 2013 Nov. Suppression of autophagy by FIP200 deletion leads to osteopenia in mice through the inhibition of osteoblast terminal differentiation. J. Bone Miner. Res. 28 (11), 2414–2430.
Liu, H.Y., Han, J., Cao, S.Y., et al., 2009 Nov 6. Hepatic autophagy is suppressed in the presence of insulin resistance and hyperinsulinemia: inhibition of FoxO1-dependent expression of key autophagy genes by insulin. J. Biol. Chem. 284 (45), 31484–31492.
Lu, X.M., Zhao, H., Wang, E.H., 2013 Apr. A high-fat diet induces obesity and impairs bone acquisition in young male mice. Mol. Med. Rep. 7 (4), 1203–1208.

Masini, M., Bugliani, M., Lupi, R., et al., 2009 Jun. Autophagy in human type 2 diabetes pancreatic beta cells. Diabetologia 52 (6), 1083–1086.
McCarthy, A.D., Etcheverry, S.B., Bruzzone, L., et al., 1997 May. Effects of advanced glycation end-products on the proliferation and differentiation of osteoblast-like cells. Mol. Cell. Biochem. 170 (1–2), 43–51.
Mizushima, N., Yoshimori, T., 2007 Nov. How to interpret LC3 immunoblotting. Autophagy 3 (6), 542–545.
Noda, T., Ohsumi, Y., 1998 Feb 13. Tor, a phosphatidylinositol kinase homologue, controls autophagy in yeast. J. Biol. Chem. 273 (7), 3963–3966.
Nollet, M., Santucci-Darmanin, S., Breuil, V., et al., 2014. Autophagy in osteoblasts is involved in mineralization and bone homeostasis. Autophagy 10 (11), 1965–1977.
Nunez, C.E., Rodrigues, V.S., Gomes, F.S., et al., 2013 Mar. Defective regulation of adipose tissue autophagy in obesity. J Obes (Lond)]–>Int. J. Obes. 12.
Onal, M., Piemontese, M., Xiong, J., et al., 2013 Jun 14. Suppression of autophagy in osteocytes mimics skeletal aging. J. Biol. Chem. 288 (24), 17432–17440.
O'Rourke, R.W., 2009 Mar. Inflammation in obesity-related diseases. Surgery 145 (3), 255–259.
Ost, A., Svensson, K., Ruishalme, I., et al., 2010 Jul. Attenuated mTOR signaling and enhanced autophagy in adipocytes from obese patients with type 2 diabetes. Mol. Med. 16 (7–8), 235–246.
Rendina-Ruedy, E., Graef, J.L., Davis, M.R., et al., 2015 Jun 10b. Strain differences in the attenuation of bone accrual in a young growing mouse model of insulin resistance. J. Bone Miner. Metab. [E Pub Ahead of Print].
Rendina-Ruedy, E., Hembree, K.D., Sasaki, A., et al., 2015a. A comparative study of the metabolic and skeletal response of C57BL/6J and C57BL/6N mice in a diet-induced model of type 2 diabetes. J. Nutr. Metab. 2015, 758080.
Sarbassov, D.D., Ali, S.M., Sabatini, D.M., 2005 Dec. Growing roles for the mTOR pathway. Curr. Opin. Cell Biol. 17 (6), 596–603.
Schwartz, A.V., Vittinghoff, E., Bauer, D.C., et al., 2011 Jun 1. Association of BMD and FRAX score with risk of fracture in older adults with type 2 diabetes. JAMA 305 (21), 2184–2192.
Smith, B.J., Lerner, M.R., Bu, S.Y., et al., 2006 Mar. Systemic bone loss and induction of coronary vessel disease in a rat model of chronic inflammation. Bone 38 (3), 378–386.
Tanida, I., Ueno, T., Kominami, E., 2004 Dec. LC3 conjugation system in mammalian autophagy. J Biochem Cell Biol]–>Int. J. Biochem. Cell Biol. 36 (12), 2503–2518.
Vashishth, D., 2007 Jun. The role of the collagen matrix in skeletal fragility. Curr Osteoporos Rep 5 (2), 62–66.
Wirth, M., Joachim, J., Tooze, S.A., 2013 Oct. Autophagosome formation—the role of ULK1 and Beclin1-PI3KC3 complexes in setting the stage. Semin. Cancer Biol. 23 (5), 301–309.
Xia, X., Kar, R., Gluhak-Heinrich, J., et al., 2010 Nov. Glucocorticoid-induced autophagy in osteocytes. J. Bone Miner. Res. 25 (11), 2479–2488.
Yamamoto, A., Tagawa, Y., Yoshimori, T., et al., 1998 Feb. Bafilomycin A1 prevents maturation of autophagic vacuoles by inhibiting fusion between autophagosomes and lysosomes in rat hepatoma cell line, H-4-II-E cells. Cell Struct. Funct. 23 (1), 33–42.
Yang, Y.H., Chen, K., Li, B., et al., 2013 Nov. Estradiol inhibits osteoblast apoptosis via promotion of autophagy through the ER-ERK-mTOR pathway. Apoptosis 18 (11), 1363–1375.